

Dehydration of the stratosphere

M. Schoeberl and
A. Dessler

This discussion paper is/has been under review for the journal Atmospheric Chemistry and Physics (ACP). Please refer to the corresponding final paper in ACP if available.

Dehydration of the stratosphere

M. Schoeberl¹ and A. Dessler²

¹Science and Technology Corporation, Columbia, MD, USA

²Texas A&M University, College Station, TX, USA

Received: 16 March 2011 – Accepted: 18 March 2011 – Published: 29 March 2011

Correspondence to: M. Schoeberl (mark.schoeberl@mac.com)

Published by Copernicus Publications on behalf of the European Geosciences Union.

Title Page

Abstract

Introduction

Conclusions

References

Tables

Figures

◀

▶

◀

▶

Back

Close

Full Screen / Esc

Printer-friendly Version

Interactive Discussion



Abstract

Domain filling, forward trajectory calculations are used to examine the global dehydration processes that control stratospheric water vapor. As with most Lagrangian models of this type, water vapor is instantaneously removed from the parcel to keep the relative humidity with respect to ice from exceeding saturation or a specified super-saturation value. We also test a simple parameterization of stratospheric convective moistening through ice lofting and the effect of gravity waves as a mechanism that can augment dehydration. Comparing diabatic and kinematic trajectories, we find, in agreement with previous authors, that the additional transport due to the vertical velocity “noise” in the kinematic calculation creates too dry a stratosphere and a too diffuse a water-vapor tape recorder signal compared observations. The diabatic simulations, on the other hand, produce stratospheric water vapor mixing ratios very close to that observed by Aura’s Microwave Limb Sounder. Convective moistening, which will increase stratospheric HDO, also increases stratospheric water vapor while gravity waves do the opposite. We find that while the Tropical West Pacific is the dominant dehydration location, dehydration over Tropical South America is also important. Antarctica also makes a contribution to the overall stratospheric water vapor budget by releasing very dry air into the Southern Hemisphere stratosphere following the break up of the winter vortex.

1 Introduction

The precise mechanism that controls stratospheric water vapor has eluded scientists for more than 60 years — since the publication of Brewer’s seminal paper (Brewer, 1949). However, significant progress has been made and many of the details of how air is dehydrated as it enters the stratosphere are now understood. For example, we know that most stratospheric dehydration takes place in a region called the tropical tropopause layer (TTL) (Sherwood and Dessler, 2000; Fueglistaler et al., 2009) a region that lies between the ~ 360 K potential temperature surface and the tropopause or between about 15 and 18 km in the tropics.

Dehydration of the stratosphere

M. Schoeberl and
A. Dessler

Title Page

Abstract

Introduction

Conclusions

References

Tables

Figures



Back

Close

Full Screen / Esc

Printer-friendly Version

Interactive Discussion



Dehydration of the stratosphere

M. Schoeberl and
A. Dessler

Title Page

Abstract

Introduction

Conclusions

References

Tables

Figures

◀

▶

◀

▶

Back

Close

Full Screen / Esc

Printer-friendly Version

Interactive Discussion



Simple back-trajectory calculations using analyzed winds and large-scale temperatures are able to accurately reproduce many of the details of TTL dehydration process and lower stratospheric water vapor (e.g., Fueglistaler et al., 2005; Jensen and Pfister, 2004; Gettelman et al., 2002). These simple calculations demonstrate that the zeroth-order physics governing the water vapor abundance in the TTL appears to be temperature variations along the advective path air parcels take as they move into the lower stratosphere (e.g., Mote et al., 1996; Fueglistaler et al., 2009).

The typical set-up for back trajectory calculations begins with a grid of parcels in the lower stratosphere that are subsequently advected backwards for a few months. Those parcels that reach the upper troposphere are then analyzed with regard to origin and temperature history. Depending on the length of the trajectory, however, a significant number of parcels may not be traceable back to the upper troposphere and the dehydration history of those parcels cannot be determined by the analysis. This is an important uncertainty of the back trajectory calculations, and one that has not yet been properly quantified. In addition, back trajectory calculations typically neglect at least three important processes. First, dehydration is usually set to occur at 100% relative humidity, meaning that supersaturation is not included in the analyses. Observations, however, show ice supersaturation is common in the tropics (Jensen et al., 2005). Second, temperature fluctuations not resolved by the reanalysis (e.g., from gravity waves) are also frequently not included. As shown by Jensen and Pfister (2004), these fluctuations are important for accurately reproducing TTL temperatures. And, third, ice lofting by convection is another neglected process. Observations show that convection does indeed reach up to and beyond the tropopause (Alcala and Dessler, 2002; Zipser et al., 2006; Dessler et al., 2006), and convection, which brings up HDO-rich air from the boundary layer, can also explain the observed enriched abundance of HDO in the TTL and lower stratosphere Moyer et al., 1996; Keith, 2000; Dessler et al., 2007).

Finally, there is the question of how to handle vertical advection of the parcels. Liu et al. (2010) performed an extensive study of stratospheric dehydration using domain filling back trajectory calculations. They compared results using both diabatic and

kinematic trajectory schemes and found that the diabatic trajectories were superior to the kinematic ones even when the vertical motion field from the assimilation was time-smoothed.

The main work discussed here is a domain filling forward trajectory analysis. By domain filling we mean a continuous release of parcels that results in hundreds of thousands of parcels filling the stratosphere and providing a statistically robust population for analysis. As we will discuss below, this approach avoids many of the pitfalls of the back trajectory studies, as well as allowing us to investigate issues that cannot be addressed with that traditional back-trajectory approach or with chemical-transport models. With our model, we focus on the processes that determine the water vapor content of the stratosphere.

In the next section we describe the model including the parameterizations for gravity waves, dehydration, convective moistening and methane photolysis. In Sect. 3 we describe our results. Summary and conclusions are presented in Sect. 4.

2 Model

2.1 Dynamics

All of our experiments use the Modern Era Retrospective-Analysis for Research and Applications (MERRA) (Bosilovich et al., 2008) for winds and temperatures. The MERRA assimilated data set runs from 1979 to the present using the GEOS-5 assimilation system. MERRA spatial resolution is 1/3 deg. longitude by 0.5 deg. latitude, although the wind and heating data (the sum of radiative and latent heat) set we are using has been averaged down to 1.25° by 1.25°. The MERRA model has 72 pressure levels extending from the surface to 0.1 hPa, but the wind data is reported on 42 levels. In the TTL and lower stratosphere, the winds are available at 150, 100, 70, and 50 hPa.

Because of the importance of temperature in our analyses, we use the MERRA's full resolution (both in the horizontal and vertical) temperature field. This vertical resolution

Dehydration of the stratosphere

M. Schoeberl and
A. Dessler

Title Page

Abstract

Introduction

Conclusions

References

Tables

Figures

◀

▶

◀

▶

Back

Close

Full Screen / Esc

Printer-friendly Version

Interactive Discussion



is about ~ 1 km in the TTL and lower stratosphere. Finally, all data sets used here are daily average fields rather than the 6-hourly data; this is done to make the meteorological data set a more manageable size.

We use the Bowman trajectory code (Bowman, 1993; Bowman and Carrie, 2002) that can run in either diabatic or kinematic mode. This code is significantly faster than the Goddard Trajectory Model (Schoeberl and Sparling, 1995), so it allows much longer trajectories required by this model. Temperatures are linearly time-space interpolated onto parcel positions. Parcel positions are output every 45 minutes along the trajectory. Running with ~ 500 K parcels, the Bowman code can perform a 25-year forward calculation in 4–5 days on a quad-core Unix workstation. This speed allows us to perform multiple experiments on the sensitivity of stratospheric water vapor to the level of supersaturation, gravity waves and convective moistening.

We have performed both kinematic and diabatic trajectory calculations similar to Schoeberl et al. (2003) and Liu et al. (2010). Kinematic means that the vertical coordinate is pressure and the parcels are moved using the MERRA's pressure tendency (ω) field whereas diabatic means that the model operates in isentropic coordinates and uses the net diabatic heating to move parcels across isentropes.

The model integration begins with the insertion of a base longitude-latitude parcel grid (typically $5^\circ \times 2^\circ$) at 250 hPa (~ 10 km) for the kinematic runs or at 360 K for the diabatic runs. The base grid extends from $\pm 60^\circ$ latitude and covers all longitudes. The insertion potential temperature is chosen such that it is, on average, above the level of zero net radiative heating – roughly the base of the TTL (Gettelman and Forster, 2002; Fueglistaler et al., 2009). A new base parcel grid is added to the model's parcel field each day approximating a continuous injection. Both the kinematic and diabatic models remove parcels at the end of each day if the parcel pressure is 250 hPa or higher. The assumption in this removal scheme is that these parcels have re-entered the troposphere. The very few parcels ascending above 1800 K in the diabatic model or 0.2 hPa in the kinematic model are also removed. The spatial density of the base grid controls the total number of parcels in the stratosphere. With the spatial density

Dehydration of the stratosphere

M. Schoeberl and
A. Dessler

[Title Page](#)[Abstract](#)[Introduction](#)[Conclusions](#)[References](#)[Tables](#)[Figures](#)[⏪](#)[⏩](#)[◀](#)[▶](#)[Back](#)[Close](#)[Full Screen / Esc](#)[Printer-friendly Version](#)[Interactive Discussion](#)

described above the model reaches steady-state of about ~500 K parcels. This number ensures that we will have a sufficient number of parcels in the stratosphere for a quantitative analysis.

In each case reported here, the model is started 1 January 2000 and integrated to the end of 2009. For the first two to three years, the number of parcels in the stratosphere grows. After that, the total number stabilizes. Thus we can safely compare the model results starting in 2005 with Aura MLS water vapor data.

2.2 Water vapor and dehydration

All base grid parcels are initiated with 200 ppmv water vapor, the approximate value of water vapor at 250 hPa in the tropics. The Marti and Mausberger (1993) relation is used to calculate the saturation vapor pressure with respect to ice. When the relative humidity exceeds the threshold, enough water is removed from the parcel to reduce the relative humidity (RH) to 100%. In most previous Lagrangian studies, the removal threshold has been set at 100% relative humidity; however, frequent observations of supersaturation in the TTL (Jensen et al., 2005) suggest that the actual threshold might be higher. We allow for supersaturation by allowing the threshold to exceed 100%. We do not consider re-evaporation of the condensate in the studies shown here although Liu et al. (2010) argues that the low bias in water vapor seen in their back trajectory studies could be due to neglect of the re-evaporating condensate.

2.3 Convective moistening

As mentioned above, the observed abundance of stratospheric HDO (Moyer et al., 1996; Keith et al., 2000; Johnson et al., 2001; Hanisco et al., 2007; Steinwagner et al., 2010) exceeds the amount predicted by Rayleigh fractionation, a theoretical limit derived by assuming that HDO-rich condensate formation and removal at 100% RH. One explanation for the larger than expected stratospheric HDO abundance is the direct injection and evaporation of HDO rich ice into the stratosphere through convective lofting.

Dehydration of the stratosphere

M. Schoeberl and
A. Dessler

Title Page

Abstract

Introduction

Conclusions

References

Tables

Figures

◀

▶

◀

▶

Back

Close

Full Screen / Esc

Printer-friendly Version

Interactive Discussion



As shown by Dessler et al. (2007) a small amount of the convective lofting of HDO rich ice can significantly increase the HDO concentration in the stratosphere. While we do not include HDO in our model, we do assess the effect of convective moistening on the stratospheric water vapor budget.

5 We use here the scheme developed by Dessler et al. (2007) to simulate the moistening process. To determine when and where trajectories are influenced by convection, we first derive a probability of convective influence as a function of pressure and the flux of outgoing longwave radiation (OLR) (Liebmann and Smith, 1996) using measurements of height-resolved ice-water content (IWC) from the Aura Microwave Limb
10 Sounder (MLS) (Livesey et al., 2005). Unlike Dessler et al. (2007), our probability table is a function of latitude and month, and is built from data obtained from OLR and IWC covering 2004–2010.

At specific intervals along each trajectory, we use the probability table and the parcel's pressure and collocated OLR to determine a probability for convective influence.
15 A random number generator is then used to determine whether the trajectory is actually influenced by convection at that time. For pressure <68 hPa, the probability is zero; for pressure >146 hPa, we use the 146 hPa probability.

When convection impacts a parcel, we set the parcel's relative humidity to 100% – this means that supersaturated parcels are dehydrated by convection (Jensen et al.,
20 2007). There are two adjustable parameters in this model, the frequency at which we test for convection and the maximum detrainment level. Increasing the frequency increases the probability that a parcel will be impacted by convection. For the experiments shown here we test for convection once a day. Parcels that are above the maximum detrainment level are never moistened so increasing the height of the detrainment level will moisten parcels that may have already been dehydrated at colder
25 temperatures and thus increasing the height will increase the water vapor in the stratosphere.

Dehydration of the stratosphere

M. Schoeberl and
A. Dessler

Title Page

Abstract

Introduction

Conclusions

References

Tables

Figures

◀

▶

◀

▶

Back

Close

Full Screen / Esc

Printer-friendly Version

Interactive Discussion



2.4 Gravity waves

Gravity waves can produce adiabatic temperature excursions that are unresolved by the MERRA analysis, and these temperature excursions can produce condensation and additional dehydration. Jensen and Pfister (2004) modeled the effect of gravity waves and showed that they had the potential to reduce stratospheric water vapor by ~ 0.5 ppmv or so. In the tropics, both high frequency inertial gravity waves and low frequency Kelvin and mixed Rossby gravity waves are present. Outside the tropics only the high frequency waves are common. In order to parameterize gravity wave effects we approximate the temperature amplitudes and frequencies from Table 1 of Jensen and Pfister (2004). We assume that the temperature is given by:

$$T_g = M(0.5\sin(\omega_h t + \phi_h) + 0.7\sin(\omega_l t + \phi_l)) | \text{latitude} | < 15^\circ$$

$$T_g = M(0.5\sin(\omega_h t + \phi_h)) | \text{latitude} | > 15^\circ$$

where M is an arbitrary tuning factor ($M = 1.0$ approximates the Jensen and Pfister (2004) simulation). We set $\omega_h = 1.1 \times 10^{-4} \text{ s}^{-1}$ for the high frequency wave, and $\omega_l = 2.3 \times 10^{-6} \text{ s}^{-1}$ for the low frequency wave. The phase, ϕ , is a uniformly distributed random number between 0 and 2π . This scheme reduces stratospheric water vapor ~ 0.2 ppmv for $M = 1$.

2.5 Methane photolysis

Methane photolysis is an important source of water in the upper stratosphere. We independently keep track of methane in each parcel and photolyze it using photochemical loss rates supplied from the Goddard two-dimensional model (Fleming et al., 2007); loss of each molecule of methane produces two molecules of H_2O (e.g., Wofsy et al., 1972; Dessler et al., 1994). Methane is set at 1.8 ppmv for all injected parcels.

Dehydration of the stratosphere

M. Schoeberl and
A. Dessler

Title Page

Abstract

Introduction

Conclusions

References

Tables

Figures

◀

▶

◀

▶

Back

Close

Full Screen / Esc

Printer-friendly Version

Interactive Discussion



3 Results

Table 1 gives an overview of the numerical experiments performed. All of the results are for the last few days of our 10-year integrations unless indicated otherwise. In these runs, we vary the amount of supersaturation, the presence of convective moistening (CM), gravity waves (GW) and the transport scheme (K or D). We compare our results to the global average MLS water vapor from 18–28 km for the same day (Lambert et al., 2007; Read et al., 2007). We use MLS version 3 data, which is an improvement over the validated version 2 data. The MLS limb water vapor measurements have 2–3 km vertical resolution. We note that the reported accuracy of MLS water vapor at lower stratospheric levels is 5–7% or about 0.3 ppmv.

In general, our results comparing diabatic and kinematic models are similar to those of Liu et al. (2010). We find that the kinematic models are dry biased compared to the diabatic simulations. Allowing for supersaturation increases stratospheric water vapor because some parcels will avoid being dehydrated to the ice vapor pressure. Convective moistening overall increases water vapor in the stratosphere by rehydrating parcels that have been dehydrated at colder temperatures. The gravity wave parameterization reduces the water vapor through excursions to lower temperatures. The best agreement with MLS is achieved, including reasonable simulation of the tropical tape recorder (see below), with 104% supersaturation using diabatic simulation, no gravity waves and no convective moistening. However, if we believe that convective moistening is required then we need to include gravity waves to correct for the excessive moisture. Since the MLS observations are only accurate to about 5–7% we cannot be completely quantitative on the level of convective moistening and gravity wave dehydration required to reproduce the stratospheric water vapor fields.

3.1 Parcel distribution

Figure 1 shows the distribution of parcels at the end of the 10-year diabatic integration (uniformly thinned out by a factor of 10) overlaid on the zonal mean temperature field.

Dehydration of the stratosphere

M. Schoeberl and
A. Dessler

Title Page

Abstract

Introduction

Conclusions

References

Tables

Figures

⏪

⏩

◀

▶

Back

Close

Full Screen / Esc

Printer-friendly Version

Interactive Discussion



Dehydration of the stratosphere

M. Schoeberl and
A. Dessler

Title Page

Abstract

Introduction

Conclusions

References

Tables

Figures

◀

▶

◀

▶

Back

Close

Full Screen / Esc

Printer-friendly Version

Interactive Discussion



As is usual with this kind of trajectory calculation, the parcel density decreases with altitude roughly in proportion to the atmospheric density. The parcels tend to cluster at lower altitudes where the heating rates and vertical velocities are smaller. We also note that there is a relative paucity of parcels at the high northern latitudes above about 25 km. This is the region of strong descent inside the vortex and parcels that originated at high altitudes are advected to lower altitudes. This effect is seen in the Southern Hemisphere six months earlier (not shown). Third, we also note a thicker cluster of tropical parcels between 22 and 27 km. This corresponds to the “the tropical pipe” region where air ascends relatively undisturbed producing the tropical tape recorders (Plumb, 2002). The isolation of the tropical region causes parcels to accumulate.

3.2 Kinematic vs. diabatic

The diabatic and kinematic computations give quite different results (Table 1). Model results should be independent of the transport scheme used, but as Danielson (1961) first noted, the aliasing of adiabatic gravity waves in the kinematic models creates “noise” in the vertical velocity field. MERRA omega fields are time smoothed to reduce this noise, but it is not entirely eliminated. The net result is that parcel models tend to be more dispersive than diabatic models when compared to observations, as seen by Liu et al. (2010).

The spurious vertical motion provides extra opportunities for dehydration compared with the diabatic calculation (which moves parcels vertically through net heating). With extra opportunities to encounter cold temperatures, the stratospheric humidity computed by the kinematic model is low biased.

To further illustrate the difference in the transport dynamics between the kinematic and diabatic models, we performed a short experiment where parcels at the same starting locations are advected kinematically and diabatically for 15 days starting 1 January 2005. Figure 2 shows the results of the experiment. It is evident that the kinematically advected parcels are dispersing through the stratosphere at a much more rapid rate than the diabatically advected parcels. This effect was first noted by

Schoeberl et al. (2003), and, as a result, the time smoothing of the vertical motion field was implemented in MERRA to compensate. A similar smoothing system is used with ERA-Interim data. Integrations performed by Liu et al. (2010, see their Fig. 12c) gave comparable results to our Fig. 2. Thus, despite the time smoothing, there appears to be sufficient remaining vertically velocity “noise” to produce excessive stochastic motion and affect the water vapor concentration.

Another way to compare the differences between the kinematic and diabatic models is to examine the age-of-air. Figure 3 shows the mean age for the diabatic and kinematic computations. The tropical pipe in the kinematic run is much narrower and young air extends only to about ~ 24 km vs. ~ 29 km in the diabatic case. Thus the “pipe” is more isolated in the diabatic experiment compared to the kinematic case.

Figure 4 shows the comparison at 20 km with age estimates from CO_2 and SF_6 from Waugh and Hall (2002). In both the kinematic and diabatic case the air is too old in the tropics, which suggests that the vertical motion field (or net heating) is too weak near the tropopause. This is consistent with analysis by Schoeberl et al. (2008) that showed that the vertical velocity in the GEOS-4 assimilation was too weak at 20 km by almost a factor of two compared to vertical motion fields derived from the observed water vapor tape recorder signal. If the tropical vertical motion were stronger, then the age-of-air in the tropics would be younger in better agreement with observations.

Outside the tropics, the kinematic model age for the extra-tropical lower stratospheric is too old (6 years vs. ~ 4 years observed). This means that parcels reaching the upper stratosphere in the kinematic model have a much longer residence time than parcels in the diabatic model. As Fig. 3 implies, the lack of isolation of the tropics allows parcels to recirculate in and out of the tropical upper stratosphere increasing their age.

4 Water vapor

Given the kinematic trajectory transport biases we will now generally restrict our discussion to the diabatic integrations. Figure 5 shows the D100 simulations of water and the

Dehydration of the stratosphere

M. Schoeberl and
A. Dessler

Title Page

Abstract

Introduction

Conclusions

References

Tables

Figures

◀

▶

◀

▶

Back

Close

Full Screen / Esc

Printer-friendly Version

Interactive Discussion



MLS zonal mean water vapor for the same day. Overall the agreement is within MLS measurement uncertainties, although the water vapor field in D100 is slightly lower than MLS. Both the tropical and Antarctic dry zones are well simulated. We also note that the model patch of tropical dry air at about 22 km is located at a somewhat lower altitude in the MLS observations. This dry patch is a section of the tape recorder; the previous Northern Hemisphere (NH) winter's dry TTL air that has ascended to 22 km. The altitude offset between the model and MLS implies that MERRA heating rates in the tropical lower stratosphere are slightly low biased.

Figure 6 shows comparisons of monthly mean water vapor maps for January and August for the D100 experiment at 82 hPa (~17.5 km) with MLS observations. There is overall excellent agreement between the model and the observed water vapor fields. We do note some important differences. The tropical west Pacific region is somewhat dryer than MLS observations and slightly wetter outside the tropics. On the other hand, the model has reproduced the dry region over South America which has not been discussed much in the literature. As we will show below, this is an important region of NH winter dehydration that has been previously neglected. For NH summer, the model reproduces the increase in tropical water vapor. Not only are there increases in water over the East Asia but over Central America as well.

Figure 7 shows the water vapor tape recorder (Mote et al., 1996, Schoeberl et al., 2008 and references therein) for D100, MLS and K120. The K120 simulation (Fig. 7a) shows rapid dispersal of the tape signal above ~20 km compared to MLS (Fig. 7b). D100, Fig. 7c, on the other hand, shows a coherent tape signal through the lower stratosphere although, as mentioned above, the signal is ascending too slowly. The incoherence of the K120 tape signal is consistent with the mean age plots shown in Fig. 3 where we noted that penetration of old air into the tropics from mid-latitudes would increase the age and narrow the tropical pipe. We also note that the upward moving water vapor (Fig. 7b, c) anomalies show downward bends in 2006 and 2008 near 20 km. This is the effect of the descending QBO circulation on the anomaly field, which is well reproduced in the MERRA heating rate data.

Dehydration of the stratosphere

M. Schoeberl and
A. Dessler

[Title Page](#)[Abstract](#)[Introduction](#)[Conclusions](#)[References](#)[Tables](#)[Figures](#)[Back](#)[Close](#)[Full Screen / Esc](#)[Printer-friendly Version](#)[Interactive Discussion](#)

4.1 Location of final dehydration events

Parcels moving through the TTL and lower stratosphere can dehydrate multiple times. Thus the pattern of dehydration shortly after a parcel is released is less relevant than the location of final dehydration point because it is the final dehydration event that ultimately determines the stratospheric water vapor concentration. There are multiple dehydration events within a month or so after parcel release with the parcels experiencing fewer dehydration events after words. Thus to provide a pattern of final dehydration we select parcels that are older than a year because very few of these parcels are continuing to dehydrate. In fact, we find that the final dehydration pattern does not vary much after about three months.

In Fig. 8 we show statistics of the locations of final dehydration point density for all D100 parcels. For all the diabatic experiments the dehydration locations are nearly the same. The point density is obtained in Fig. 8a by counting final dehydration locations in a $5^\circ \times 10^\circ$ latitude-longitude grid and normalizing by the total number of parcels. The altitude-latitude density pattern shown in Fig. 8b is obtained the same way using a $5^\circ \times 1.35$ km latitude-height grid.

In agreement with many previous studies, the principle dehydration region is the Tropical West Pacific (TWP), which is the coldest part of the TTL (e.g. Fueglistaler et al., 2009 and others). However, outside the TWP, Fig. 8a shows significant dehydration taking place in zones over India, Africa, South America and Antarctica. Somewhat surprising is the wide extent of dehydration over South America, and very low water vapor amounts observed by MLS and present in the model (Fig. 6a) over South America are consistent with this zone of dehydration. It is also interesting that the TWP dehydration region is split into two regions, one north of the equator extending to East Asia, and one south of the equator extending from northern Australia across eastern New Guinea. This TWP dipole dehydration distribution also shows up in the vertical distribution of dehydration locations (Fig. 8b). We have overlaid the winter temperatures in Fig. 8b to illustrate the co-location of cold temperatures and final dehydration points in the tropics and over Antarctica.

Dehydration of the stratosphere

M. Schoeberl and
A. Dessler

Title Page

Abstract

Introduction

Conclusions

References

Tables

Figures

⏪

⏩

◀

▶

Back

Close

Full Screen / Esc

Printer-friendly Version

Interactive Discussion



Dehydration of the stratosphereM. Schoeberl and
A. Dessler

Title Page

Abstract

Introduction

Conclusions

References

Tables

Figures

◀

▶

◀

▶

Back

Close

Full Screen / Esc

Printer-friendly Version

Interactive Discussion



Figure 9 shows the D100 seasonal distribution of final dehydration density for winter (December–February), spring (March–May), summer (June–August) and fall (September–November). The winter dehydration exhibits many of the features of the annual average dehydration (Fig. 8a) with the highest density of dehydration points occurring in the southern branch of the TWP dipole and with almost no contribution from East Asia. Dehydration over South America is also important in this season. The transition in spring shows that the dehydration focus is in the tropical Pacific and SE Asia. Dehydration in the summer is most common over East Asia with a smaller contribution from Antarctica. In the case of Antarctica, the major dehydration zone lies close to the Antarctic Peninsula where large-scale orographic waves that are resolved by MERRA can depress temperatures. The altitude of this zone is shown in Fig. 8b. North polar gravity wave driven dehydration is also seen in the model, but to a much lesser extent than in the Southern Hemisphere. During NH winter this dehydration mostly occurs over the Scandinavian Peninsula. In the NH fall, dehydration over Antarctica occurs as does dehydration over S. America and the N. Australia-New Guinea region.

Table 2 shows how each region in Figs. 8a and 9 contributes to the control of water vapor in the stratosphere in percent and in average water vapor mixing ratio. The percent is of number model parcels (over a year old) that dehydrated in the specified region shown in the Fig. 8a map.

As is evident in Figs. 8a and 9 and Table 2, in NH winter the TWP is the predominant locus of dehydration of the stratosphere; however, as noted above, the next most important zone for dehydration is the continent of South America. Water vapor amounts from these zones are about 4 ppmv. In NH summer, dehydration events over India (and east Asia) are most important, but dehydration over Antarctica plays a role as well. During NH summer, the water vapor mixing ratio for parcels that dehydrated over Antarctica average 2 ppmv whereas all other regions the average is ~5–6 ppmv.

The Antarctic stratosphere reaches minimum temperatures during a period when the polar vortex is very isolated (Schoeberl and Hartmann, 1991) and thus the dry air inside the vortex cannot easily circulate into the Southern Hemisphere until the vortex break

up in November. Therefore, despite the very dry air being released by the Antarctic vortex, the net contribution of Antarctica to stratospheric dehydration is still smaller than the overall contribution from the tropics.

Tracking parcels after final dehydration and sorting their distribution as a function of altitude and latitude allows us to further explore the role of the various dehydration zones in controlling stratospheric water vapor. Using the parcel positions, we can show the relative distribution of parcels that have dehydrated in different regions. Figure 10 amplifies the results from Table 2 by showing the vertical distribution of the fraction of parcels as a function of latitude-height that dehydrated in each region – we refer to these fractional maps as “Influence.” We neglect the Northern Hemisphere influence since it is negligible in all seasons and we lump South America and Africa together.

Table 2 and Fig. 10 shows that the TWP influence dominates the stratosphere but that South America and Africa together are important regions for dehydration in NH winter. During the NH summer the influence of TWP is still higher than India (and East Asia) despite the fact that the water vapor maximum is clearly located over India (Fig. 6b). Figure 10b shows that, during Antarctic winter, the vortex confines the dehydration to regions south of $\sim 60^\circ$ S. After the breakup of the vortex (early NH winter), the influence of Antarctic appears to be reduced to the region below 18 km (Fig. 10a) where a weak vortex persists. Despite the strong dehydration in the Antarctic stratosphere, the overall influence is small. As a side note, the kinematic integrations show much wider influence of the Antarctic region in the Southern Hemisphere (not shown). This wider Antarctic influence in the kinematic model occurs because diffusive parcel exchange across the vortex wall allows more air to be processed by the cold Antarctic stratosphere locating the final dehydration points there.

5 Summary and conclusion

This paper describes the results from a domain filling, forward trajectory model that has been used to examine the dehydration processes that control stratospheric water

Dehydration of the stratosphere

M. Schoeberl and
A. Dessler

Title Page

Abstract

Introduction

Conclusions

References

Tables

Figures



Back

Close

Full Screen / Esc

Printer-friendly Version

Interactive Discussion



Dehydration of the stratosphere

M. Schoeberl and
A. Dessler

Title Page

Abstract

Introduction

Conclusions

References

Tables

Figures

◀

▶

◀

▶

Back

Close

Full Screen / Esc

Printer-friendly Version

Interactive Discussion



vapor. We use the MERRA assimilated winds and temperatures in these calculations. Comparing diabatic and kinematic trajectories, we find that the kinematic trajectory results are significantly different from the diabatic calculations. Despite vertical velocity time smoothing of the MERRA data, the additional stochastic transport due to the vertical velocity “noise” in the kinematic calculation creates too dry a stratosphere and a too diffuse a tape recorder signal compared observations. The reason the kinematic stratosphere is too dry is because the random motions of parcels provide a higher probability for encountering cold temperatures and thus more dehydration. These results are in agreement with the study by Liu et al. (2010).

The diabatic calculations provide more reasonable transport, and the mean age for the diabatic calculation better matches to the observations. Comparisons to MLS water vapor data show that the diabatic simulation of stratospheric water vapor assuming dehydration at ice saturation is only slightly dry, and the water vapor tape recorder signal compares well to MLS observations although the ascent of the tape signal is too slow.

We explore the effects of changing the super-saturation, including convective moistening and gravity wave induced temperature fluctuations. We can match the MLS observations if we assume super-saturation of about 104%. Alternatively, we can obtain the same agreement with MLS measurements if we include both convective moistening and gravity waves, setting the saturation at 100%. Convective moistening increases stratospheric water vapor and gravity wave temperature fluctuations reduce it. Thus, if we believe that convective moistening must be present to reproduce HDO measurements, (Moyer et al., 1996; Keith, 2000; Dessler et al., 2007) then gravity waves are also required to provide additional dehydration. Future simulations will focus on simultaneously matching H₂O and HDO in the stratosphere.

The model allows us to quantify the spatial pattern of final dehydration locations. Although we find that the TWP dominates the dehydration processes in winter, South America is also important, and this regions show up in the MLS H₂O observations as well. Antarctica makes an additional contribution to the Southern Hemisphere water

vapor budget by releasing very dry air into the Southern Hemisphere stratosphere following the break up of the winter vortex, but its influence is not great. The India-East Asia region is important for dehydration during NH summer, but it is not as important as TWP.

- 5 *Acknowledgements.* A. Dessler acknowledges NASA Aura grant NNX08AR27G to Texas A&M University and K. Bowman for help on the trajectory code.

References

- Alcala, C. M. and Dessler, A. E.: Observations of deep convection in the tropics using the TRMM precipitation radar, *J. Geophys. Res.*, 107, 4792, doi:10.1029/2002JD002457, 2002.
- 10 Bosilovich, M. G., Chen, J., Robertson, F. R., and Adler, R. F.: Evaluation of global precipitation in reanalyses, *J. Appl. Meteor. Climatol.*, 47, 2279–2299, doi:10.1175/2008JAMC1921.1, 2008.
- Bowman, K. P.: Large-scale isentropic mixing properties of the Antarctic polar vortex from analyzed winds, *J. Geophys. Res.*, 98, 23013–23027, 1993.
- 15 Bowman, K. P. and Carrie, G. D.: The mean-meridional transport circulation of the troposphere in an idealized GCM, *J. Atmos. Sci.*, 59, 1502–1514, 2002.
- Brewer, A. W.: Evidence for a world circulation provided by the measurements of helium and water vapour distribution in the stratosphere, *Q. J. Roy. Meteor. Soc.*, 75, 351–363, 1949.
- Corti, T., Luo, B. P., de Reus, M., et al.: Unprecedented evidence for deep convection hydrating the tropical stratosphere, *Geophys. Res. Lett.*, 35, L10810, doi:10.1029/2008gl033641, 2008.
- 20 Danielsen, E. F.: Trajectories – isobaric, isentropic and actual, *J. Meteorol.*, 479–486, 1961.
- Dessler, A. E.: The effect of deep, tropical convection on the tropical tropopause layer, *J. Geophys. Res.*, 107, 4033, doi:10.1029/2001JD000511, 2002.
- 25 Dessler, A. E., Weinstock, E. M., Hintsa, E. J., Anderson, J. G., Webster, C. R., May, R. D., Elkins, J. W., and Dutton, G. S.: An examination of the total hydrogen budget of the lower stratosphere, *Geophys. Res. Lett.*, 21, 2563–2566, 1994.
- Dessler, A. E., Hintsa, E. J., Weinstock, E. M., Anderson, J. G., and Chan, K. R.: Mechanisms

Dehydration of the stratosphere

M. Schoeberl and
A. Dessler

Title Page

Abstract

Introduction

Conclusions

References

Tables

Figures

◀

▶

◀

▶

Back

Close

Full Screen / Esc

Printer-friendly Version

Interactive Discussion



Dehydration of the stratosphere

M. Schoeberl and
A. Dessler

Title Page

Abstract

Introduction

Conclusions

References

Tables

Figures

◀

▶

◀

▶

Back

Close

Full Screen / Esc

Printer-friendly Version

Interactive Discussion



controlling water vapor in the lower stratosphere: A tale of two stratospheres, *J. Geophys. Res.*, 100, 23, 167–123, 172, 1995.

Dessler, A. E., Palm, S. P., and Spinhirne, J. D.: Tropical cloud-top height distributions revealed by the Ice, Cloud, and Land Elevation Satellite (ICESat)/Geoscience Laser Altimeter System (GLAS), *J. Geophys. Res.*, 111, D12215, doi:10.1029/2005JD006705, 2006.

Dessler, A. E., Hanisco, T. F., and Fueglistaler, S. A.: Effects of convective ice lofting on H₂O and HDO in the tropical tropopause layer, *J. Geophys. Res.*, 112, D18309, doi:10.1029/2007JD008609, 2007.

Fleming, E. L., Jackman, C. H., Weisenstein, D. K., and Ko, M. K. W.: The impact of inter-annual variability on multidecadal total ozone simulations, *J. Geophys. Res.*, 112, D10310, doi:10.1029/2006JD007953, 2007.

Fueglistaler, S., Bonazzola, M., Haynes, P. H., and Peter, T.: Stratospheric water vapor predicted from the Lagrangian temperature history of air entering the stratosphere in the tropics, *J. Geophys. Res.*, 110, D08107, doi:10.1029/2004JD005516, 2005.

Fueglistaler, S., Dessler, A. E., Dunkerton, T. J., Folkins, I., Fu, Q., and Mote, P. W.: The tropical tropopause layer, *Rev. Geophys.*, RG1004, doi:10.1029/2008RG000267, 2009.

Gettelman, A. and de Forster, P. M. F.: A climatology of the tropical tropopause layer, *J. Meteorol. Soc. Jpn.*, 80, 911–942, 2002.

Gettelman, A., Randel, W. J., Wu, F., and Massie, S. T.: Transport of water vapor in the tropical tropopause layer, *Geophys. Res. Lett.*, 29(1), 1009, doi:10.1029/2001GL013818, 2002.

Hanisco, T., Moyer, E. J., Weinstock, E. M., St. Clair, J. M., Sayres, D. S., Smith, J. B., Lockwood, R., Anderson, J. G., Dessler, A. E., Keutsch, F. N., Spakman, J. R., Read, W. G., and Bui, T. P.: Observations of deep convective influence on stratospheric water vapor and its isotopic composition, *Geophys. Res. Lett.*, 34, L04814, doi:10.1029/2006GL027899, 2007.

Jensen, E. J. and Pfister, L.: Transport and freeze-drying in the tropical tropopause layer, *J. Geophys. Res.*, D02207, doi:10.1029/2003JD004022, 2004.

Jensen, E. J., Smith, J. B., Pfister, L., Pittman, J. V., Weinstock, E. M., Sayres, D. S., Herman, R. L., Troy, R. F., Rosenlof, K., Thompson, T. L., Fridlind, A. M., Hudson, P. K., Cziczo, D. J., Heymsfield, A. J., Schmitt, C., and Wilson, J. C.: Ice supersaturations exceeding 100% at the cold tropical tropopause: implications for cirrus formation and dehydration, *Atmos. Chem. Phys.*, 5, 851–862, doi:10.5194/acp-5-851-2005, 2005.

Jensen, E. J., Ackerman, A. S., and Smith, J. A.: Can overshooting convection dehydrate the tropical tropopause layer?, *J. Geophys. Res.*, 112, D11209, doi:10.1029/2006JD007943,

Dehydration of the stratosphere

M. Schoeberl and
A. Dessler

Title Page

Abstract

Introduction

Conclusions

References

Tables

Figures

◀

▶

◀

▶

Back

Close

Full Screen / Esc

Printer-friendly Version

Interactive Discussion

2007.

Johnson, D. G., Jucks, K. W., Traub, W. A., and Chance, K. V.: Isotopic composition of stratospheric water vapor: Implications for transport, *J. Geophys. Res.*, 106, 12, 219–212, 226, 2001.

5 Keith, D. W.: Stratosphere-Troposphere exchange: Inferences from the isotopic composition of water vapor, *J. Geophys. Res.*, 105, 15167–15173, 2000.

Lambert, A., Read, W. G., Livesey, N. J., et al.: Validation of the Aura Microwave Limb Sounder middle atmosphere water vapor and nitrous oxide measurements, *J. Geophys. Res.*, 112, D24S36, doi:10.1029/2007JD008724, 2007.

10 Liebmann, B. and Smith, C. A.: Description of a complete (interpolated) outgoing longwave radiation data set, *B. Am. Meteorol. Soc.*, 77, 1275–1277, 1996.

Liu, Y. S., Fueglistaler, S., and Haynes, P.: Advection-condensation paradigm for stratospheric water vapor, *J. Geophysical Res.*, 115, D24307, doi:10.1029/2010JD014352, 2010.

Marti, J. and Mauersberger, K.: A survey and new measurements of ice vapor pressure at temperatures between 170 K and 250 K, *Geophys. Res. Lett.*, 20, 363–366, 1993.

15 Mote, P. W., Rosenlof, K. H., McIntyre, M. E., Carr, E. S., Gille, J. C., Holton, J. R., Kinnerson, J. S., Pumphrey, H. C., Russell, III, J. M., and Waters, J. W.: An atmospheric tape recorder: The imprint of tropical tropopause temperatures on stratospheric water vapor, *J. Geophys. Res.*, 101, 3989–4006, 1996.

20 Moyer, E. J., Irion, F. W., Yung, Y. L., and Gunson, M. R.: ATMOS stratospheric deuterated water and implications for troposphere-stratosphere transport, *Geophys. Res. Lett.*, 23, 2385–2388, 1996.

Plumb, R. A.: Stratospheric Transport, *J. Meteor. Soc. Japan*, 80, 793–809, 2002.

25 Read, W. G., Lambert, A., Bacmeister, J., et al.: Aura Microwave Limb Sounder upper tropospheric and lower stratospheric H₂O and relative humidity with respect to ice validation, *J. Geophys. Res.*, 112, D24S35, doi:10.1029/2007JD008752, 2007.

Rosenlof, K. H. and Reid, G. C.: Trends in the temperature and water vapor content of the tropical lower stratosphere: Sea surface connection, *J. Geophys. Res.*, 113, D06107, doi:10.1029/2007JD009109, 2008.

30 Rosenlof, K. H., Oltmans, S. J., Kley, D., et al.: Stratospheric water vapor increases over the past half-century, *Geophys. Res. Lett.*, 28, 1195–1198, 2001.

Schoeberl, M. R. and Hartmann, D.: The Dynamics of the Polar Vortex, *Science*, 251, 46–52, 1991.

Dehydration of the stratosphere

M. Schoeberl and
A. Dessler

Title Page

Abstract

Introduction

Conclusions

References

Tables

Figures

◀

▶

◀

▶

Back

Close

Full Screen / Esc

Printer-friendly Version

Interactive Discussion



- Schoeberl, M. R. and Sparling, L.: Trajectory Modeling, in: Diagnostic Tools in Atmospheric Physics, edited by: Fiocco, G. and Visconti, G., Proceedings of the International School of Physics “Enrico Fermi”, 124, 289–306, 1995.
- 5 Schoeberl, M., Douglass A., Zhu Z., and Pawson, S.: A comparison of the lower stratospheric age spectra derived from a general circulation model and two data assimilation systems, *J. Geophys. Res.*, 108, D3, 4113, doi:10.1029/2002JD002652, 2003.
- Schoeberl, M. R., Douglass, A. R., Newman, P. A., et al.: QBO and annual cycle variations in tropical lower stratosphere trace gases from HALOE and Aura MLS observations, *J. Geophys. Res.*, 113, D05301, doi:10.1029/2007jd008678, 2008.
- 10 Schoeberl, M. R., Douglass, A. R., Stolarski, R. S., Pawson, S., Strahan, S. E., and Read, W.: Comparison of lower stratospheric tropical mean vertical velocities, *J. Geophys. Res.*, 113, D24109, doi:10.1029/2008JD010221, 2008.
- Sherwood, S. C. and Dessler, A. E.: On the control of stratospheric humidity, *Geophys. Res. Lett.*, 27, 2513–2516, 2000.
- 15 Steinwagner, J., Fueglistaler, S., Stiller, G., von Clarmann, T., Kiefer, M., Boorsboom, P. P., van Delden, A., and Rockmann, T.: Tropical dehydration processes constrained by the seasonality of stratospheric deuterated water, *Nature Geosci.*, 3, 262–266, doi:10.1038/NGEO822, 2010.
- Waugh, D. W. and Hall, T. M.: Age of stratospheric air: Theory, observations, and models, *Rev. Geophys.*, 40(4), 1010, doi:10.1029/2000RG000101, 2002.
- 20 Wofsy, S. C., McConnell, J. C., and McElroy, M. B.: Atmospheric CH₄, CO, and CO₂, *J. Geophys. Res.*, 77, 4477–4493, 1972.
- Zhou, X. L., Geller, M. A., and Zhang, M. H.: Cooling trend of the tropical cold point tropopause temperatures and its implications, *J. Geophys. Res.*, 106, 1511–1522, 2001.
- 25 Zipser, E. J., Cecil, D. J., Liu, C., Nesbitt, S. W., and Yorty, D. P.: Where are the most intense thunderstorms on Earth?, *B. Am. Meteorol. Soc.*, 87, 1057–1071, 2006.

Dehydration of the stratosphere

M. Schoeberl and
A. Dessler

Table 2. Dehydration statistics by region.

Location	All Seasons (100%)		NH Winter (30%)		NH Summer (24%)	
	%	H ₂ O	%	H ₂ O	%	H ₂ O
West Pacific	41	4.2	52	3.4	36	5.2
India	11	4.6	5	3.9	20	5
South America	21	4.5	26	3.8	10	6
Africa	10	4.4	15	4.1	3	5.8
Antarctica	16	2.2	0	–	30	2.0
Northern Hemisphere	1	5.8	~0	–	1	–

Statistics of final dehydration locations for regions shown in Fig. 8a (D100). Percent shows the total percentage of model parcels that dehydrated in the indicated region. H₂O is the average water vapor mixing ratio (ppmv) for parcels that dehydrated in that location. Only parcels over a year old are considered.

[Title Page](#)
[Abstract](#)
[Introduction](#)
[Conclusions](#)
[References](#)
[Tables](#)
[Figures](#)
[Back](#)
[Close](#)
[Full Screen / Esc](#)
[Printer-friendly Version](#)
[Interactive Discussion](#)


Dehydration of the stratosphereM. Schoeberl and
A. Dessler

Title Page

Abstract

Introduction

Conclusions

References

Tables

Figures

◀

▶

◀

▶

Back

Close

Full Screen / Esc

Printer-friendly Version

Interactive Discussion

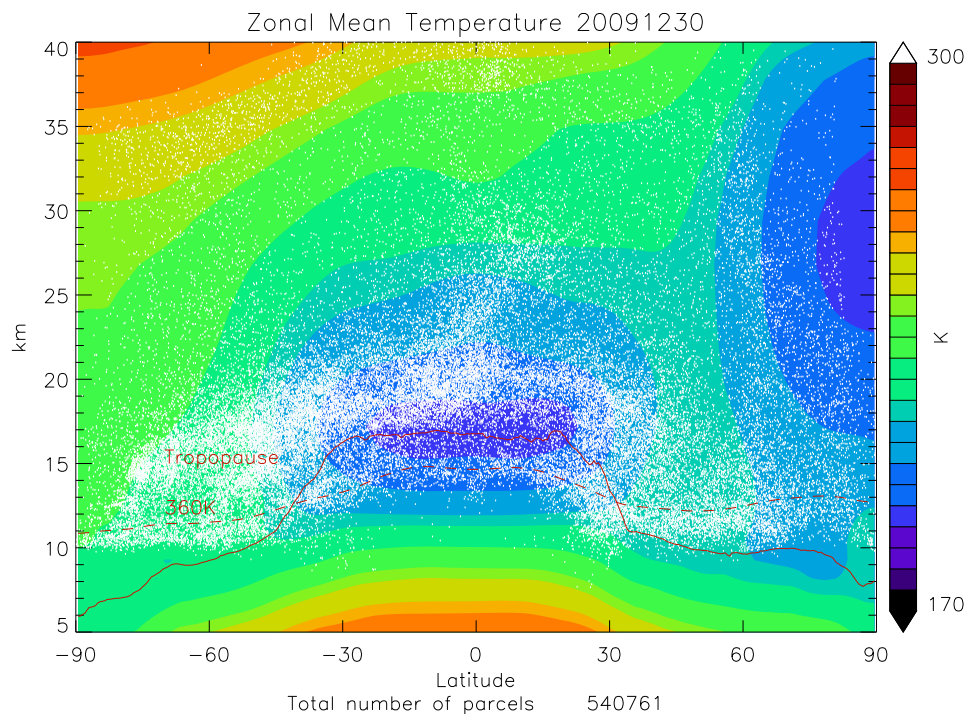


Fig. 1. Parcel distribution for diabatic experiment on 30 December 2009 thinned by a factor of 10 for visibility. Injection began 1 January 2000. Colors show the zonal mean temperature distribution from MERRA. Red lines identify the zonal mean 360 K and tropopause levels. Parcels moving below about 10 km are eliminated. The total number of parcels is 527 951.

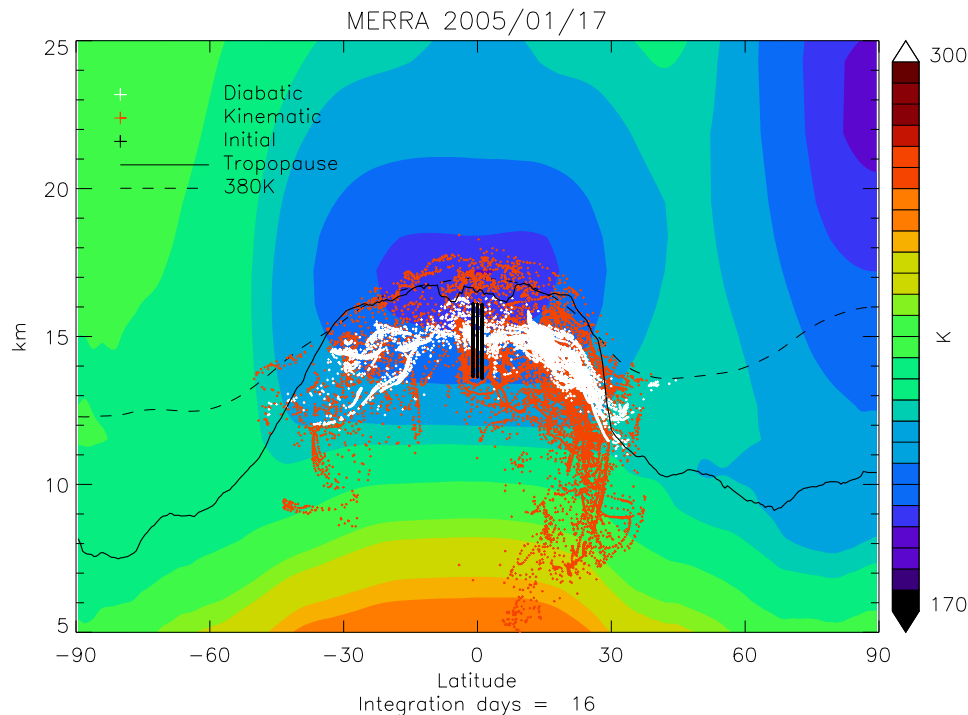
Dehydration of the stratosphereM. Schoeberl and
A. Dessler

Fig. 2. Results from a 16 day advection experiment using diabatic (white) and kinematic (orange) trajectory techniques. Parcels are initiated in black box region in the center of the figure. Note that the kinematic trajectory parcels are dispersing more rapidly than the diabatically advected parcels. Background image is average temperature over this period.

Title Page

Abstract

Introduction

Conclusions

References

Tables

Figures

◀

▶

◀

▶

Back

Close

Full Screen / Esc

Printer-friendly Version

Interactive Discussion



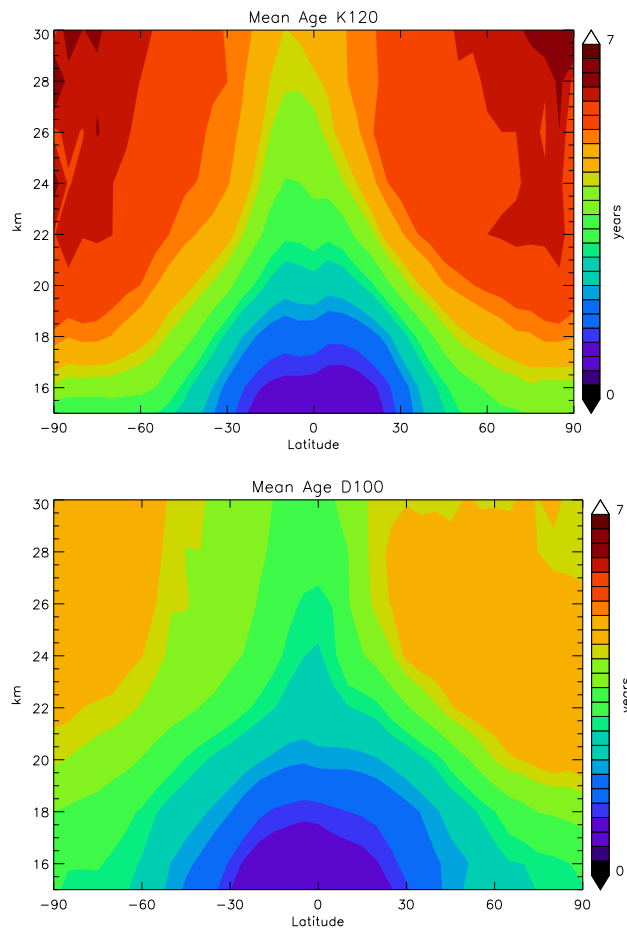


Fig. 3. Left, mean age for a kinematic trajectory run. Right mean age for a diabatic trajectory run.

Dehydration of the stratosphere

M. Schoeberl and
A. Dessler

Title Page

Abstract Introduction

Conclusions References

Tables Figures

◀ ▶

◀ ▶

Back Close

Full Screen / Esc

Printer-friendly Version

Interactive Discussion



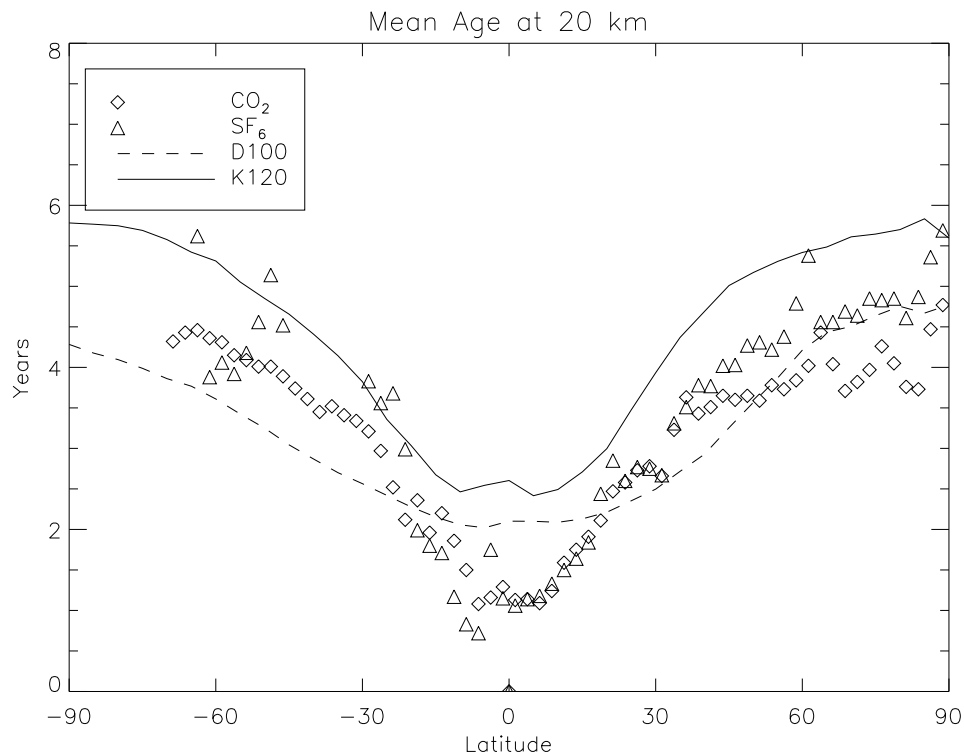
Dehydration of the stratosphereM. Schoeberl and
A. Dessler

Fig. 4. Mean age averaged over a 2009 at 20 km with measurements based on CO₂ and SF₆ from Waugh and Hall (2002). Solid line, kinematic integration; dashed line, diabatic integration.

Title Page

Abstract

Introduction

Conclusions

References

Tables

Figures

◀

▶

◀

▶

Back

Close

Full Screen / Esc

Printer-friendly Version

Interactive Discussion



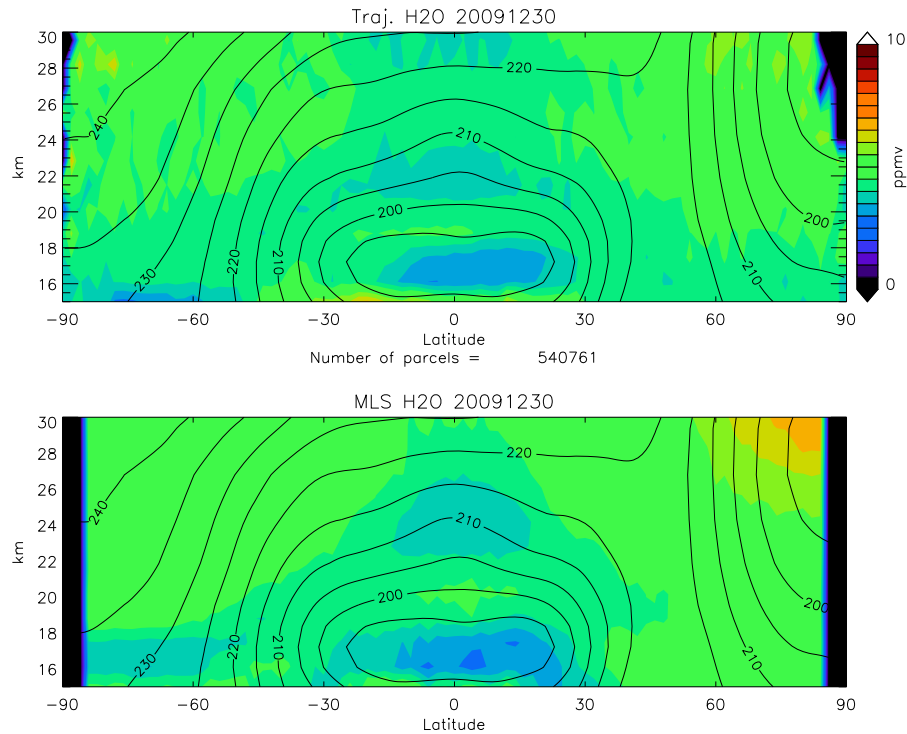
Dehydration of the stratosphereM. Schoeberl and
A. Dessler

Fig. 5. MZonal mean water vapor concentration at the end of the particle integrations. Top D100 (Diabatic, 100% supersaturation) experiment, bottom MLS V3 observations (see Table 1). Zonal mean temperatures are shown as black contours. Temperature data are from MERRA.

Title Page

Abstract

Introduction

Conclusions

References

Tables

Figures

◀

▶

◀

▶

Back

Close

Full Screen / Esc

Printer-friendly Version

Interactive Discussion



Dehydration of the stratosphere

M. Schoeberl and
A. Dessler

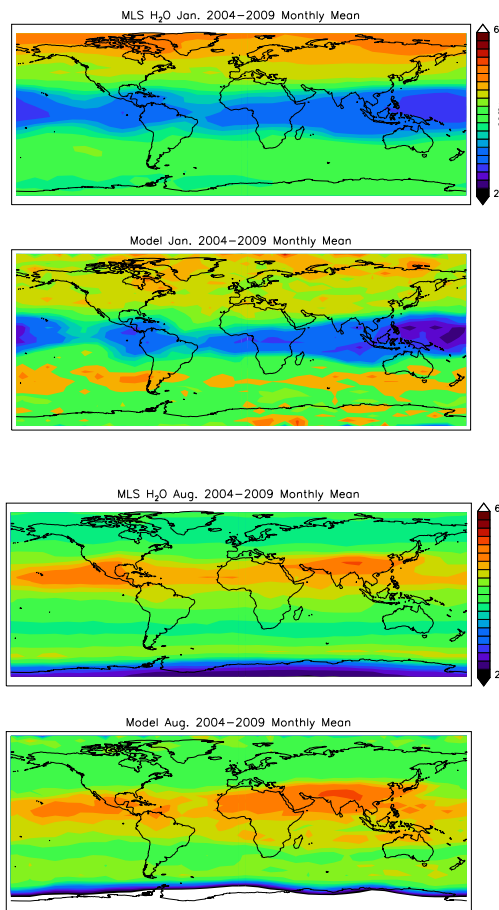
[Title Page](#)[Abstract](#)[Introduction](#)[Conclusions](#)[References](#)[Tables](#)[Figures](#)[◀](#)[▶](#)[◀](#)[▶](#)[Back](#)[Close](#)[Full Screen / Esc](#)[Printer-friendly Version](#)[Interactive Discussion](#)

Fig. 6. Monthly mean water vapor at 82 hPa (~ 17.5 km) for January (Part **a**, top) and August 2005–2009 (Part **b**, bottom) for the model and MLS; D100 experiment.

Dehydration of the stratosphere

M. Schoeberl and
A. Dessler

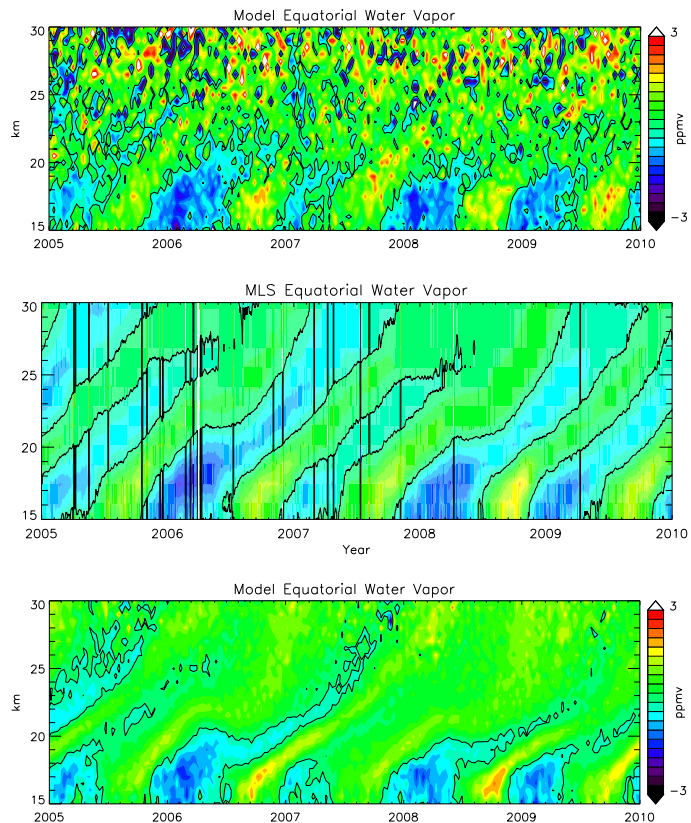
[Title Page](#)[Abstract](#)[Introduction](#)[Conclusions](#)[References](#)[Tables](#)[Figures](#)[◀](#)[▶](#)[◀](#)[▶](#)[Back](#)[Close](#)[Full Screen / Esc](#)[Printer-friendly Version](#)[Interactive Discussion](#)

Fig. 7. Water vapor concentration anomalies at the equator vs. time. Part (a) (top) K120 (kinematic) experiment, middle, Part (b) (middle) MLS V3 observations, Part (c) (bottom) D104 (diabatic) experiment (see Table 1).

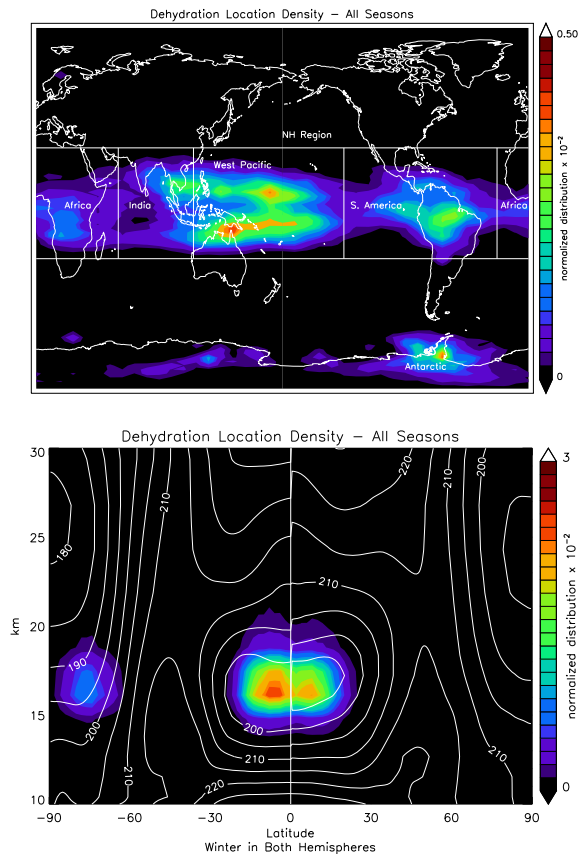


Fig. 8. Upper plot (part **a**) shows horizontal distribution of final dehydration location density for all parcels more than 1 year old, regardless of when they were dehydrated (from the D100 run). The lower plot (part **b**) shows the annual vertical distribution of dehydration locations along with the winter zonal mean temperature contours superimposed (winter in the SH and winter in the NH).

Dehydration of the stratosphere

M. Schoeberl and
A. Dessler

Title Page

Abstract

Introduction

Conclusions

References

Tables

Figures

◀

▶

◀

▶

Back

Close

Full Screen / Esc

Printer-friendly Version

Interactive Discussion



Dehydration of the stratosphere

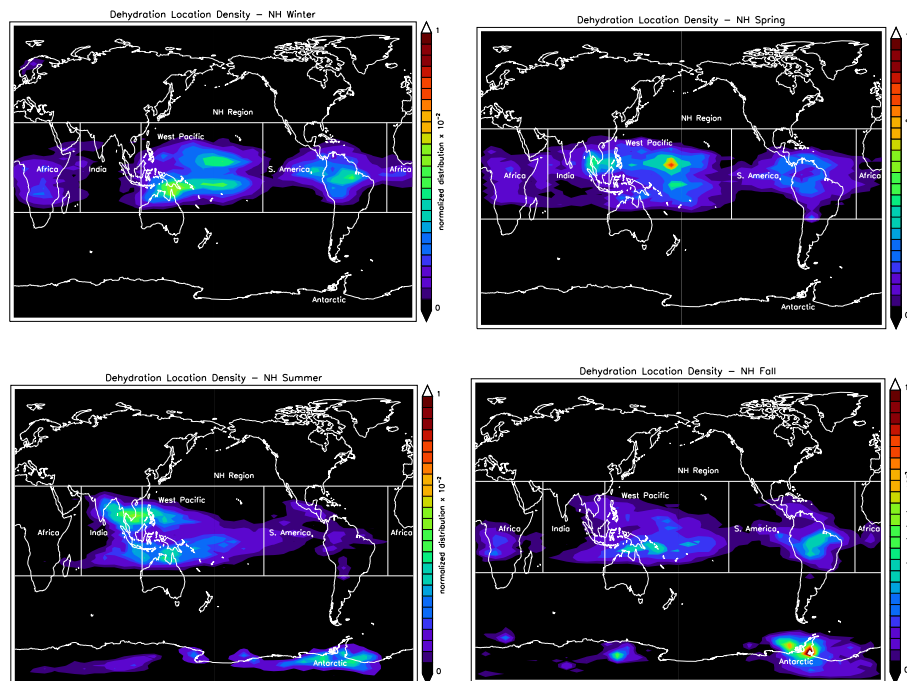
M. Schoeberl and
A. Dessler

Fig. 9. Density of final dehydration points by season as shown in Fig. 8a. Upper left **(a)**, winter, upper right **(b)**, spring, lower left **(c)**, summer, lower right **(d)**, fall.

Title Page

Abstract

Introduction

Conclusions

References

Tables

Figures

◀

▶

◀

▶

Back

Close

Full Screen / Esc

Printer-friendly Version

Interactive Discussion



Dehydration of the stratosphere

M. Schoeberl and
A. Dessler

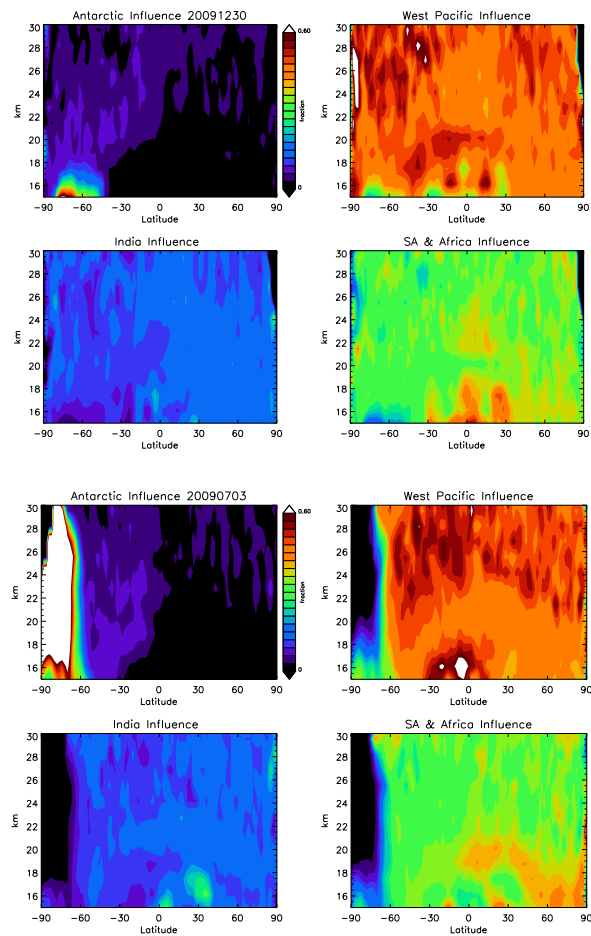
[Title Page](#)[Abstract](#)[Introduction](#)[Conclusions](#)[References](#)[Tables](#)[Figures](#)[⏪](#)[⏩](#)[◀](#)[▶](#)[Back](#)[Close](#)[Full Screen / Esc](#)[Printer-friendly Version](#)[Interactive Discussion](#)

Fig. 10. Fraction of parcels from different locations in the stratosphere for 31 December 2009 (part a, top) and 3 July 2009 (part b, bottom), D100. Figure 8a shows the region map labels.